Ultrafast dynamics at the zinc phthalocyanine/zinc oxide nanohybrid interface for efficient solar light harvesting in the near red region

Zaki S. Seddigi [a], Saleh A. Ahmed [b],[*], Samim Sardar [c], Samir Kumar Pal [c],[**]

[a] Department of Environmental Health, Faculty of Public Health and Health informatics, Umm Al-Qura University, 21955 Makkah, Saudi Arabia
[b] Chemistry Department, Faculty of Applied Sciences, Umm Al-Qura University, 21955 Makkah, Saudi Arabia
[c] Department of Chemical, Biological and Macromolecular Sciences, S.N. Bose National Centre for Basic Sciences, Block JD, Sector III, SaltLake, Kolkata 700 098, India

ARTICLE INFO

ABSTRACT

Phthalocyanine-based light harvesting nanomaterials are attractive due to their low cost, eco-friendly properties and sensitivity in the red region of the solar spectrum. However, for any practical application, phthalocyanines need to be chemically modified for anchoring groups with wide-band semiconducting nanomaterials. In this paper, zinc phthalocyanine (ZnPc) was functionalized with two carboxyl groups containing a biologically important ligand, tartrate, using a facile wet chemistry route and duly sensitized zinc oxide (ZnO) to form nanohybrids for application in photocatalytic devices. The nanohybrids have been characterized using a high-resolution transmission/scanning electron microscope (HRTEM, FEG-SEM), X-ray diffraction (XRD), steady-state infrared/UV–vis absorption and emission spectroscopy for their structural details and optical properties, whereas the ultrafast dynamical events, which are key for understanding the photocatalytic activities, were monitored using picosecond resolution fluorescence techniques. More specifically, vibrational spectroscopy (FTIR) revealed the covalent connection of ZnPc with the host ZnO nanoparticles via the tartrate ligand. The efficiency of the material for photocatalysis under red light irradiation was found to be significantly enhanced compared to bare ZnO. A mechanistic pathway for the formation of photo-induced reactive oxygen species (ROS) in an aqueous medium for the photocatalytic efficacy was investigated. To make a prototype for a potential application in a flow device for water decontamination, we have sensitized ZnO nanorods (ZnO NR) with tartrate-functionalized ZnPc. The molecular proximity of ZnPc to the ZnO surface has been confirmed by picosecond resolution Förster Resonance Energy Transfer (FRET) from the intrinsic emission of surface defects of ZnO NR to the attached ZnPc. The excited-state electron transfer dynamics, as revealed by a picosecond resolution fluorescence study (TCSPC), is in good agreement with the enhanced charge separation at the interface of the nanohybrid. The enhanced photoresponse, wavelength-dependent photocurrent of the sensitized nanorods and photodegradation of a model water pollutant in a prototype device format confirmed the potential use of the nanohybrids in water purification.

1. Introduction

The choice of photo-sensitizers in solar light-harvesting applications, including dye sensitized solar cells (DSSC) and visible light photocatalysis (VLP) is very important. In most cases, polypyridyl ruthenium complexes are likely choices for such applications [1–4]. While the complexes work reasonably well in visible light, the main drawback of such complexes is a lack of reasonable absorption in the near-IR region. Given that IR energy accounts for 49% of the solar spectrum, an extended red response of the sensitizers is necessary to improve the device efficiency [5]. Phthalocyanines (PCs) have been used in light-harvesting applications, including in polymer-based hybrid DSSC [6], to complement the optical absorption of the polymer in the red region of the solar spectrum. The chemical structures of the PCs are characterized by an aromatic monocyclic ligand carrying clouds of delocalized π-conjugated electrons and a central metallic atom with typically 2+ oxidation states playing the role of electron donor to the ligands. Zinc phthalocyanines (ZnPc) are a class of PCs whose main electronic features are explained in detail using DFT [7] and are represented schematically in Fig. 1. ZnPc is usually modified by the addition of anchoring groups for light-harvesting applications [8–13].
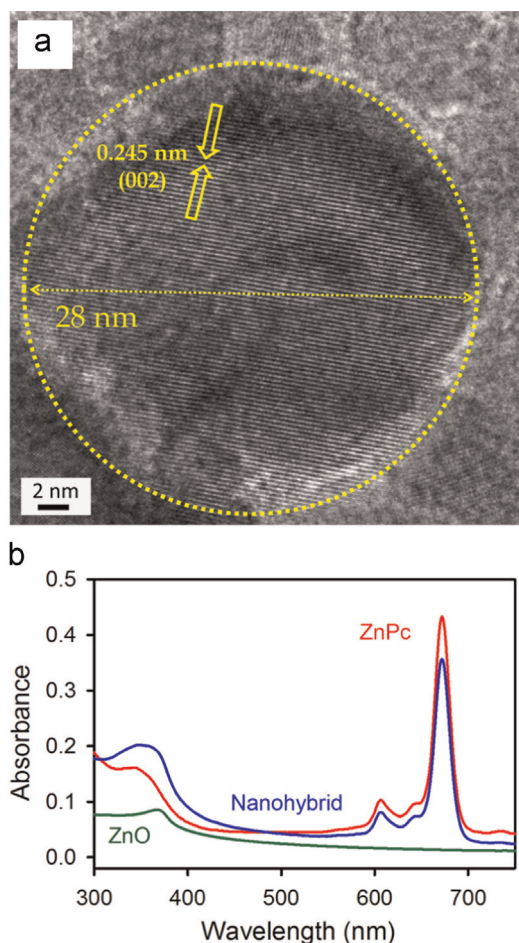
Fig. 1. (a) High-resolution transmission electron microscopy (HRTEM) of ZnO NP. Inter-fringe distance of 0.245 nm is consistent with (002) planes of the ZnO crystal. (b) UV–vis absorption spectra of ZnPc in DMSO and the nanohybrid are shown. The absorption spectrum of the suspended NPs without sensitization is shown for comparison.

In this manuscript, a facile means to attach a biologically important ligand, tartrate, to the central metal of ZnPc using simple wet chemistry was employed. We have made nanohybrids of tartrate-functionalized ZnPc with zinc oxide (ZnO) of different morphologies (particles and nanorods) for light-harvesting applications or red light photocatalysis. Although titania (TiO_2) was reported to be a more efficient charge separator from the excited sensitizer in light harvesting, recently DSSC based on ZnO have attained efficiency that is comparable to titania [6]. Moreover, ZnO has emerged more recently in the framework of light-harvesting devices as an alternative to titania because of its flexibility in materials synthesis and significant electron mobility [14]. While Fourier transform infrared (FTIR) spectroscopy reveals attachment of the tartrate ligand through a carboxylate end to the ZnO NP, X-ray diffraction (XRD) confirms the intactness of the crystal structure of ZnO upon functionalization with tartrate. We have also studied the photocatalytic activity of the nanohybrid under red light illumination with a model water pollutant, methyl orange (MO), and found significant enhancement, which is found to be a manifestation of enhanced ROS formation from the nanohybrid in aqueous solution. To use the functional material (nanohybrid) in a flow device for the decontamination of polluted water, we have used ZnO nanorods (ZnO NR) on a glass plate duly functionalized with tartrate–ZnPc. The intrinsic emission of the ZnO NR and its spectral overlap with the absorption spectrum of ZnPc reveals Förster Resonance Energy Transfer (FRET) from the surface of the NR to the attached ZnPc, confirming the close proximity between the sensitizer ZnPc to the host ZnO NR. We have confirmed enhanced photocurrent under visible light and measured the wavelength-dependent photocurrent in the sensitized ZnO NR. A prototype of the flow device has also been made and tested for potential application in decontamination of the model water pollutant (MO).

2. Experimental section

2.1. Reagents

Zinc acetate dihydrate, ZnO ($\sim$30 nm), methyl orange, zinc phthalocyanine (ZnPc), tartaric acid, zinc nitrate hexahydrate, and hexamethylenetetramine were purchased from Sigma-Aldrich. All compounds were of the highest commercially available purity and used as received. Ultrapure water (Millipore System, 18.2 MΩ cm) and ethanol ($\geq$99% for HPLC, purchased from Sigma-Aldrich) were used as solvents. Analytical-grade chemicals were used for synthesis without further purification. Dimethyl sulfoxide (DMSO) and sodium hydroxide (NaOH) were purchased from Merck.
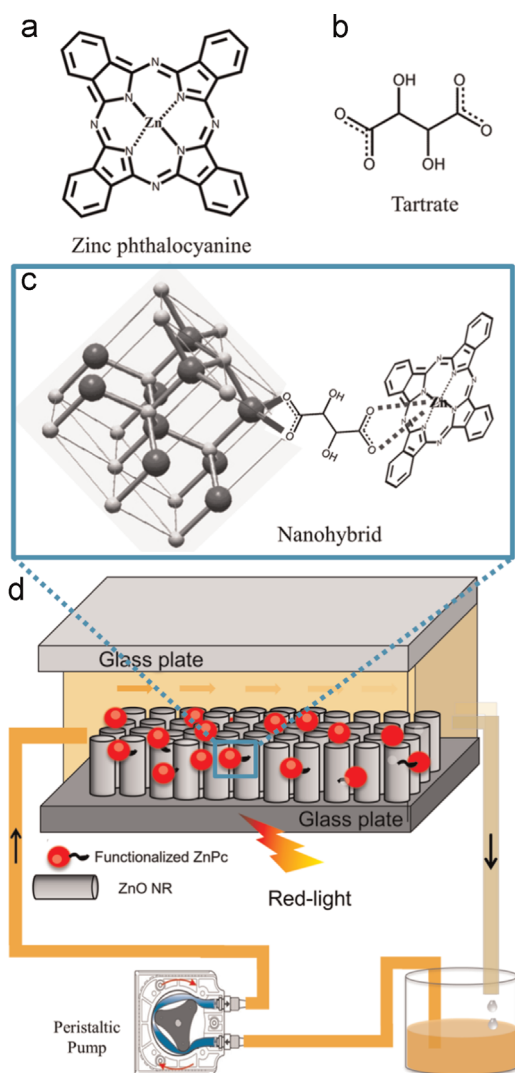
Scheme 1. (a, b) Molecular structure of the sensitizer zinc phthalocyanine (ZnPc) and the ligand tartrate are shown. (c) The nanohybrid: possible molecular attachment of ZnPc with ZnO crystal through the tartrate ligand is indicated. (d) Schematic of the prototype flow device using the nanohybrid as the functional material is shown.
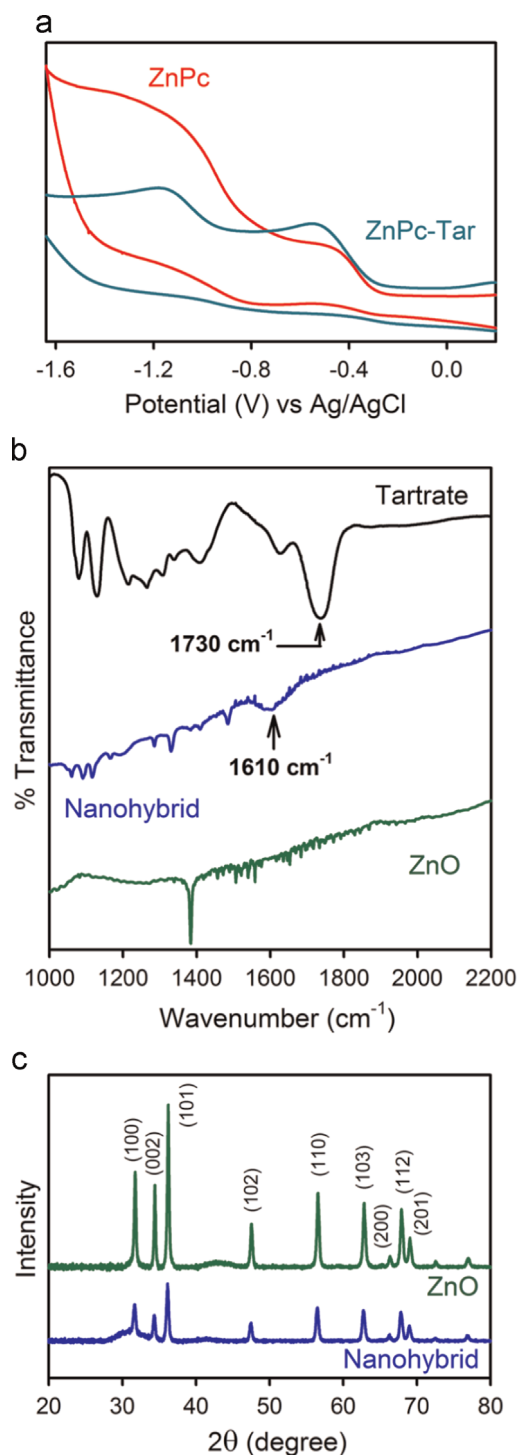
Fig. 2. (a) Cyclic voltammograms of ZnPc (red) and ZnPc attached to tartrate ligands (ZnPc–Tar, dark cyan). The CVs were measured in DMSO-aqueous KOH solution at 0.1 V s^{-1} scan rate and Ag/AgCl as reference electrode. (b) FTIR of the nanohybrid, ZnO NPs and tartrate are shown. A bidentate binding of the tartrate to the ZnO through the carboxylate end is evident (see text). (c) X-ray diffractograms of the nanohybrid and reference ZnO NPs are shown. Intactness of crystal structure of ZnO in the nanohybrid is evident (see text). (For interpretation of the references to color in this figure legend, the reader is referred to the web version of this article.)

2.2. Sensitization of ZnPc on the ZnO NP surface through tartrate ligands

Tartrate has been chosen over other potential organic molecules, including citrate and L-serine, as a ligand for the following reason. The

yield of the ligand-functionalized ZnPc is found to be highest in the case of tartrate, as is evident from the following experiment. The three ligands in the aqueous phase and ZnPc in chloroform were stirred for 12 h. Then, the aqueous phase was separated and emission of the ZnPc was monitored upon excitation at 633 nm. The concentration of the complex in the aqueous phase was maximum for the tartrate-containing solution, indicating the strongest binding between tartrate and ZnPc among the three ligands. A 0.5 mM ZnPc (C$_{32}$H$_{16}$N$_8$Zn) solution was prepared in dimethyl sulfoxide (DMSO) with constant stirring for 1 h. The functionalization of ZnO NPs with tartrate ligands was carried out at room temperature in dark ambience by adding ZnO NPs into a 0.5 mM tartrate aqueous solution (pH adjusted to 9 by NaOH) with continuous stirring for 6 h. Then, the tartrate-functionalized ZnO NPs were added to the 0.5 mM ZnPc solution in a dimethyl sulfoxide (DMSO)–deionized (DI) water (1:1, v–v) mixture and stirred for 12 h under dark conditions. After the sensitization process, the solution was centrifuged for a few minutes and the supernatant clear solution of unattached dyes was removed. Then, the sensitized material was washed with a DMSO–water mixture several times to remove any unattached dye. The nanohybrid was then dried in a water bath and stored in the dark until further use.

2.3. Synthesis of ZnO NRs

Zinc acetate dihydrate, Zn(CH$_3$COO)$_2$ 2H$_2$O (Merck), zinc nitrate hexahydrate, Zn(NO$_3$)$_2$, 6H$_2$O (Sigma-Aldrich), hexamethylenetetramine, C$_6$H$_{12}$N$_4$ (Aldrich) were used as the starting materials for a low temperature hydrothermal synthesis of ZnO NRs on FTO substrates. Detailed processes for the hydrothermal growth of single-crystal ZnO NRs are described in our previous reports [15–17]. In brief, a ZnO seed layer was initially deposited on cleaned glass substrates by the spray-pyrolysis method at 100 °C using 10 mM zinc acetate solution in isopropanol. The seeded glass substrates were then annealed in air at 350 °C for 5 h and used for the hydrothermal growth of the ZnO NRs. An aqueous solution of zinc nitrate (20 mM) and hexamethylenetetramine (20 mM) was used as the precursor solution for the ZnO NR growth, which was carried out at 90 °C for 40 h. This led to the growth of ZnO NRs with a length of approximately 2–3 μm and diameter of 80–100 nm. To maintain a constant growth rate of the ZnO NRs during the hydrothermal process, the old precursor solution was replaced with a fresh solution every 1 h. The as-obtained ZnO NR samples were then taken out of the reaction vessel and rinsed thoroughly with DI water to remove unreacted residues. Finally, the samples were annealed in air at 350 °C for 1 h prior to the study.

2.4. Sensitization of ZnPc on the ZnO NR surface through tartrate ligands

The functionalization of ZnO NRs with tartrate ligands was carried out at room temperature in the dark by immersing the glass plates with ZnO NRs into a 0.5 mM tartrate aqueous solution (pH adjusted to 9 by NaOH) for 12 h. After that, the plates were washed with distilled water several times. For ZnPc sensitization, a 0.5 mM ZnPc solution, C$_{32}$H$_{16}$N$_8$Zn, was prepared in dimethyl sulfoxide (DMSO) with constant stirring for 1 h. The sensitization of the ZnO NRs with ZnPc dye was carried out in darkness at room temperature by dipping the ZnO NR samples into the prepared dye solution for 12 h. After the sensitization process, the ZnO NRs were extracted from the dye solution, rinsed with a DMSO–water mixture thoroughly (to remove any physisorbed dye molecules), and stored in darkness for further use.

2.5. Characterization methods

Field Emission Scanning Electron Microscopy (FESEM, QUANTA FEG 250) was used to investigate the surface morphology of the
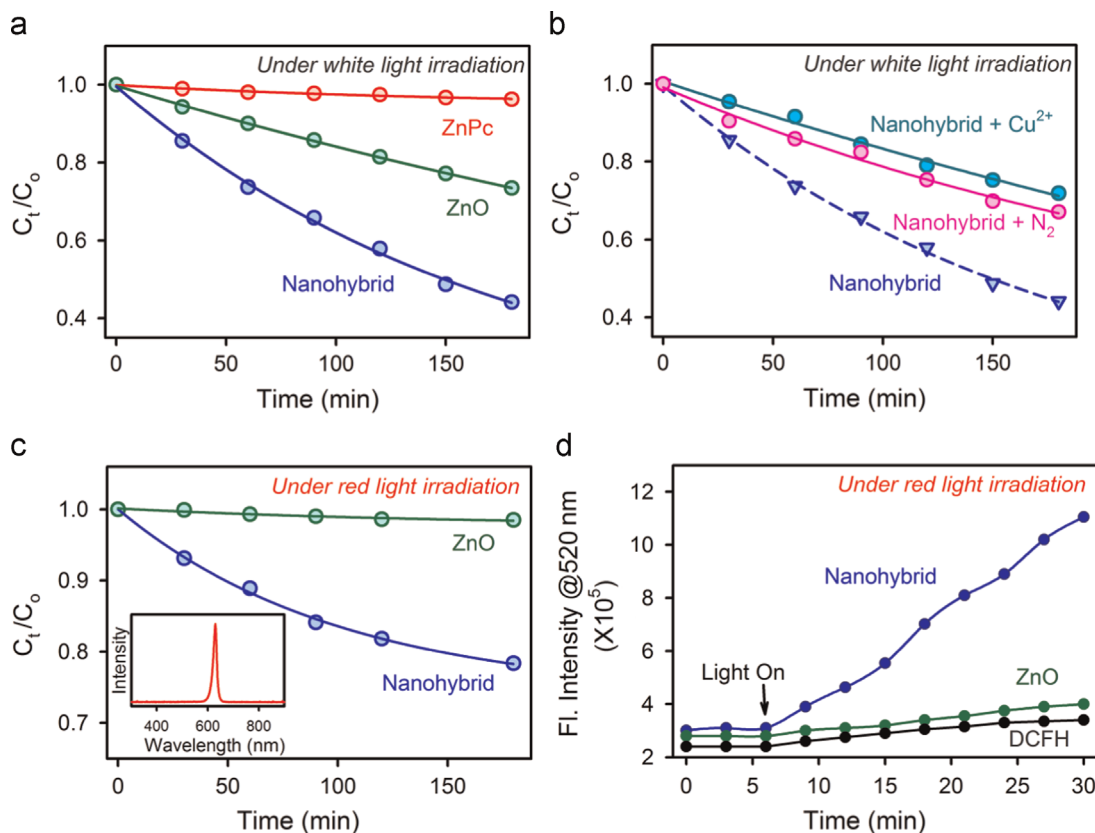
Fig. 3. (a) Methyl orange (MO) photodegradation in the presence of the nanohybrid and comparison with bare ZnO NP under white light illumination are shown. (b) Decrease in the rate of MO photodegradation in the presence of Cu^{2+} and after N_2 purging compared to that of the nanohybrid alone. (c) Photocatalytic activity of the nanohybrid under red light (optical irradiance spectrum is in the inset) illumination is shown. The reference for bare ZnO NPs does not show any activity under red light. (d) Red light-induced reactive oxygen species (ROS) generation in the presence of nanohybrid and comparison with ZnO and control (DCFH) in aqueous solution are shown.

samples. Transmission electron microscopy (TEM) was carried out using an FEI (Technai S-Twin) instrument with an acceleration voltage of 200 kV. A drop of sample was placed on a carbon-coated copper grid and particle sizes were determined from micrographs recorded at a high magnification of 100,000 ×. Electrochemical experiments were performed using a CH analyzer potentiostat (CHI1110C). For cyclic voltammetry, a three electrode system consisting of a glassy carbon working electrode, a platinum counter electrode and a reference electrode was employed. All the potentials reported in this paper are referenced to the Ag/Ag^+ couple and performed in DMSO-1 (M) aqueous KOH solution. X-ray diffraction (XRD) was used to characterize the crystal phase using a PANalytical XPERTPRO diffractometer equipped with Cu Kα radiation (at 40 mA and 40 kV) at a scanning rate of $0.02° \, s^{-1}$ in the 2θ range from 20° to 80°. Fourier transform infrared spectra (FTIR) were obtained with a JASCO FTIR-6300 spectrometer by the KBr Pellet method. For optical experiments, the steady-state absorption and emission were recorded with a Shimadzu UV-2600 spectrophotometer and a Jobin Yvon Fluoromax-3 fluorimeter, respectively. Picosecond resolution spectroscopic studies were carried out using a commercial time correlated single photon counting (TCSPC) setup from Edinburgh Instruments (instrument response function, IRF=80 ps, excitation at 375 nm, 409 nm and 633 nm). The details of the experimental setup and methodology were described in our earlier report [18,19]. The average lifetime (amplitude-weighted) of a multi-exponential decay is expressed as $\tau_{av} = \sum_{i=1}^{N} c_i \tau_i$, where c_i's are weighted percentages with time constants of τ_i's. The Förster Resonance Energy Transfer (FRET) has been studied between donor (ZnO) and acceptor (ZnPc) by following traditional methodology [20,21] by calculating the Förster

distance (R_0 in Å)

$$R_0 = 0.211 \times [\kappa^2 n^{-4} Q_D J]^{\frac{1}{6}} \tag{1}$$

where κ^2 is a factor describing the relative orientation in space of the transition dipoles of the donor and acceptor and the magnitude is assumed to be 2/3. The refractive index (n) of the medium is considered to be 1.496. Q_D, the integrated quantum yield of the donor in the absence of acceptor, is measured to be 3.8×10^{-3}. J, the overlap integral, which expresses the degree of spectral overlap between the donor emission and the acceptor absorption, is given by

$$J(\lambda) = \frac{\int_0^\infty F_D(\lambda) \varepsilon_A(\lambda) \lambda^4 d\lambda}{\int_0^\infty F_D(\lambda) d\lambda} \tag{2}$$

where $F_D(\lambda)$ is the fluorescence intensity of the donor in the wavelength range of λ to $\lambda + d\lambda$ and is dimensionless; $\varepsilon_A(\lambda)$ is the extinction coefficient (in $M^{-1} \, cm^{-1}$) of the acceptor at λ. If λ is in nm, then J is in units of $M^{-1} \, cm^{-1} \, nm^4$. The donor–acceptor distance (r_{DA}) can be easily calculated using the formula,

$$r_{DA}^6 = \frac{[R_0^6 (1 - E)]}{E} \tag{3}$$

Here, E is the efficiency of energy transfer. The transfer efficiency is measured using the relative fluorescence lifetime of the donor, in absence (τ_D) and presence (τ_{DA}) of the acceptor.

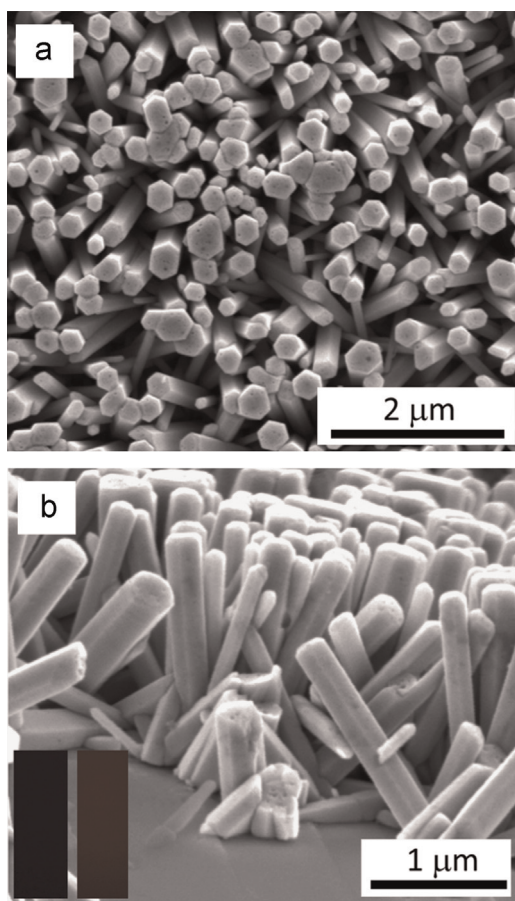$$E = 1 - \frac{\tau_{DA}}{\tau_D} \tag{4}$$

Fig. 4. (a, b) FEG-SEM of the ZnO nanorods (ZnO NR) on a glass plate for the prototype flow device is shown. Fluorescent micrographs of the plate before and after ZnPc sensitization are also shown in the inset of (b).

From the average lifetime calculation for the nanohybrid, we obtain the effective distance between the donor and the acceptor (r_{DA}) using the above equations.

2.6. Photocatalytic tests

The photocatalytic activity of the nanohybrid under UV–vis light illumination has been tested for photodecomposition of methyl orange (MO, taken as a model pollutant) in water. The photodegradation reaction of MO (initial concentration $C_0 = 0.3 \times 10^{-4}$ M) was carried out in a 10 mm optical path quartz cell reactor containing 3.5 mL of a model solution with a concentration of 1 g L^{-1} of the nanohybrid. The suspension was irradiated with a red LED (50 W) and also with a xenon lamp (300 W) for UV–vis light, and an appropriate number of aliquots was collected from the reactor at different time intervals. The percentage degradation (%DE) of MO was determined using equation 5

$$\% \, DE = \frac{I_0 - I}{I_0} \times 100$$

(5)

where I_0 is the initial absorbance of MO at $\lambda_{max} = 460$ nm and I is the absorbance of MO after light irradiation.

2.7. Photocurrent under white light illumination and wavelength-dependent photocurrent measurements

Photocurrent measurements were conducted in the device geometry described earlier [18,22]. For the measurement, platinum NPs

deposited on FTO substrates were used as counter electrodes. The platinum (Pt) NPs were deposited on the FTO substrates by thermal decomposition of a 5 mM platinum chloride, H$_2$PtCl$_6$, H$_2$O, and Fluka solution in isopropanol at 385 °C for 30 min. Nanohybrids were used as the photoelectrode and the two electrodes were placed on top of each other with a single layer of 50-μm-thick surlyn 1702 (Dupont) as a spacer between the two electrodes. A liquid electrolyte (1 M KCl) was used as the hole conductor and filled in the inter-electrode space by using capillary force, through two small holes (diameter = 1 mm) pre-drilled on the counter electrode. Finally, the two holes were sealed using another piece of surlyn to prevent leakage of the electrolyte. In all of our experiments, the active area of light exposure was fixed at 1 cm^2. The wavelength-dependent photocurrent is measured using a homemade setup with a Bentham monochromator and dual light (tungsten and xenon) sources.

3. Results and discussion

The chemical structure of zinc phthalocyanine (ZnPc), tartrate ligand and a possible binding site for the formation of the nanohybrid are shown in Scheme 1. A typical high-resolution transmission electron microscopic (HR-TEM) image of ZnO NPs is shown in Fig. 1a. The lattice fringe of ZnO NP shows an interplanar distance of ~0.245 nm, corresponding to the spacing between two (002) planes [23]. The average particle size is estimated to be ~28 nm. Fig. 1b shows the UV–vis absorption spectra of ZnPc in DMSO and the nanohybrids. The absorption spectrum of the suspended ZnO NPs is also shown in Fig. 1b as a reference. The intactness of the optical spectrum of ZnPc in the nanohybrid is confirmed from the studies.

In order to investigate the attachment of the tartrate ligand to the ZnPc, cyclic voltammetry experiments were performed as shown in Fig. 2a. Two observed redox processes are associated with ring based processes, Zn(II)Pc^{2-}/Zn(II)Pc^{3-} and Zn(II)Pc^{3-}/Zn(II)Pc^{4-} as ZnPc complexes are not known to show redox activity at the central metal [24]. The redox potentials ($E_{1/2}$) of ZnPc are 0.62 V and 1.26 V vs Ag/AgCl in DMSO-1 (M) aqueous KOH solution for Zn(II)Pc^{2-}/Zn(II)Pc^{3-}, Zn(II)Pc^{3-}/Zn(II)Pc^{4-} couples, respectively. Whereas the $E_{1/2}$ values of ZnPc attached to tartrate ligand (ZnPc–Tar) are shifted to 0.68 V and 1.30 V, respectively. The shift in the redox potentials can be attributed to the binding of tartrate ligand at the axial position of the ZnPc [25]. The Fourier transform infrared (FTIR) technique is used to investigate the binding mode of the carboxylate group of the tartrate on the ZnO NP surface because the attachment is very crucial for efficient binding of ZnPc and eventually for light-harvesting applications. For free tartrate, stretching frequencies of the carboxylic group are at 1730 cm^{-1} and 1412 cm^{-1} for antisymmetric and symmetric stretching vibrations, respectively, as shown in Fig. 2b. When tartrate is attached to ZnO, the stretching frequencies of the carboxylic group are located at 1630 cm^{-1} and 1478 cm^{-1} for antisymmetric and symmetric stretching vibrations, respectively. The shifting of the stretching frequencies clearly indicates the formation of a covalent bond between the ligand tartrate and the host ZnO NPs [22]. The difference between the carboxylate stretching frequencies, $\Delta = \nu_{as} - \nu_{sym}$ is useful in identifying the bonding mode of the carboxylate ligand [26]. The observed Δ value for the hybrid material is 152 cm^{-1}, which is smaller than that of free tartrate (318 cm^{-1}). This observation reveals that the binding mode of tartrate on the ZnO surface is predominantly bidentate. The XRD study (Fig. 2c) on the bare ZnO NPs (2θ range from 20° to 70°) and upon sensitization with tartrate-functionalized ZnPc shows characteristic planes of wurzite ZnO, (100), (002), (101), (102), (110), (103), (200), (112) and (201). The intactness of the crystal planes of ZnO upon sensitization with tartrate–ZnPc is also clear from the study. It has to be noted that (002) planes are more polar than (100) and (101) planes. Mclaren et al. [27]
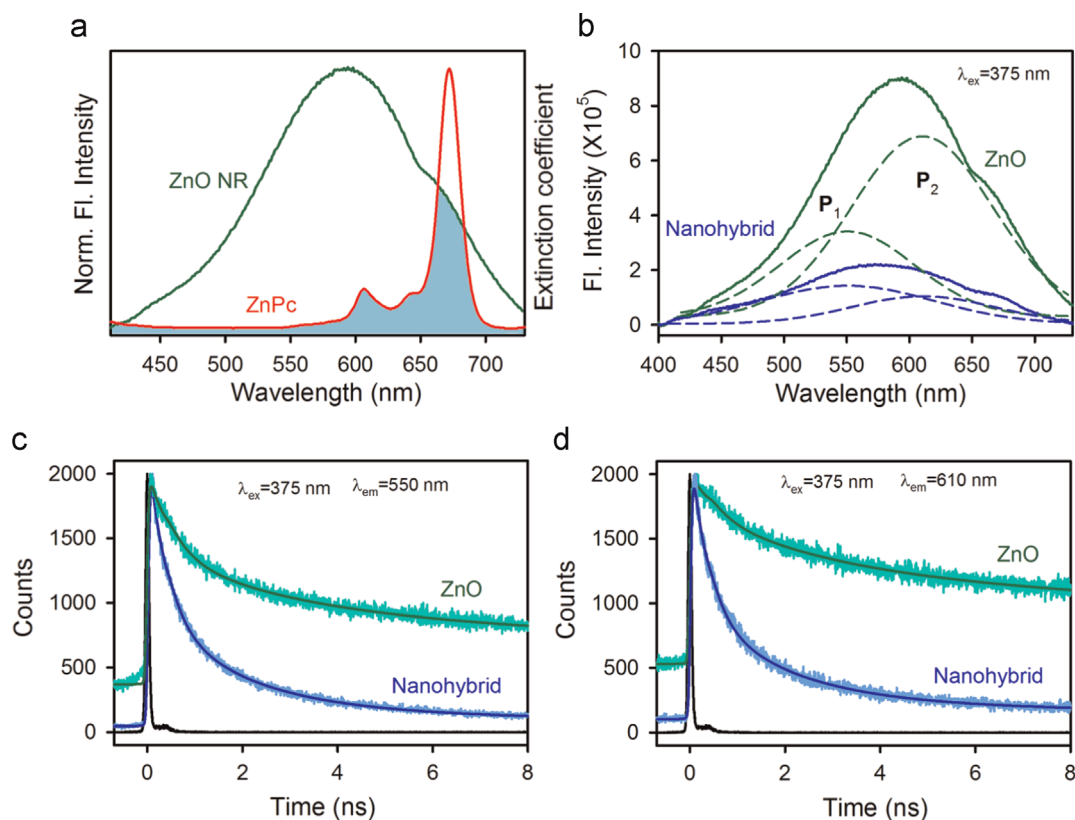
Fig. 5. (a) Spectral overlap of the emission of ZnO NR and the absorption spectrum of ZnPc is shown. (b) Emission from ZnO NRs. Deconvolution of the emission into two peaks (P$_1$ and P$_2$) is also shown. Relatively higher quenching of P$_2$ in the nanohybrid compared to bare ZnO NR is evident. (c, d) picosecond resolved emission transients of ZnO NR and nanohybrid detected at 550 nm (P$_1$ position) and 610 nm (P$_2$ position), respectively. Higher quenching efficiency for P$_2$ is consistent with steady-state spectra shown in (b).

Table 1
Dynamics of picosecond-resolved luminescence transients of ZnPc and the nanohybrid[a].

Sample	Excitation wavelength (nm)	Detection wavelength (nm)	τ_1 (ns)	τ_2 (ns)	τ_3 (ns)	τ_{av} (ns)
ZnO NR	375	550	0.40 (42.5%)	2.70 (27.6%)	31.70 (29.9%)	10.40
Nanohybrid	375	550	0.30 (61.3%)	1.75 (32.3%)	10.60 (6.4%)	1.40
ZnO NR	375	610	0.40 (28.6%)	2.75 (30.9%)	31.70 (40.5%)	13.80
Nanohybrid	375	610	0.30 (62.7%)	1.80 (32.2%)	14.00 (5.1%)	1.50
ZnPc	633	680	3.40 (100%)			3.40
Nanohybrid	633	680	0.05 (93%)	3.10 (7%)		0.25

[a] Numbers in parentheses indicate relative weights.

have shown that the terminal polar faces are more active surfaces for photocatalysis than the nonpolar surfaces perpendicular to them.

Fig. 3a shows the results of the investigation of photocatalytic efficiency of the nanohybrid under white light irradiation ($\lambda > 365$ nm) in an aqueous environment. The test water under investigation contains methyl orange (MO) and the model water contaminant. From the experimental data, a significant enhancement of the photocatalytic efficiency in the case of nanohybrids compared to that of the bare ZnO is clearly evident. During photocatalytic reaction, photoinduced electrons and holes escape recombination and migrate to the semiconductor surface which consequently generates (in the presence of oxygen and water) highly oxidative radicals, that can degrade the organic pollutants. In order to investigate the role of reactive oxygen species (ROS), the photocatalysis experiments were performed after N$_2$ purging for 1 h which drives out the dissolved oxygen. The decrease in the photocatalytic activity as shown in Fig. 3b confirms that the mechanism is mainly through ROS [28]. The photocatalysis rate also decreases in the presence of Cu^{2+} which is a well-known

scavenger of super oxides and photogenerated electrons [29,30]. The photocatalytic efficiency of the nanohybrid under red light illumination (620 nm) is also monitored, as shown in Fig. 3c. The nanohybrid exhibits enhanced photocatalytic activity under red light as the sensitizer absorbs in the same region, whereas bare ZnO NPs show no activity under red light because of the lack of absorption in the visible or near infrared region. Comparison with the bare sensitizer ZnPc is difficult to make because the sensitizer is completely insoluble in water. The quantum yield (No of contaminant molecules reacted per incident photon) of the methyl orange degradation reaction in the presence of nanohybrid under white and red light irradiation is found to be 7.0×10^{-6} and 4.6×10^{-6}, respectively. The quantum yield values are consistent with the reported literature for methyl orange degradation [31] by dye-sensitized TiO$_2$ nanoparticles under visible light irradiation through ROS pathway. Our observation is consistent with the enhanced photocatalytic activity of other nanohybrids reported in the literature [18,32,33]. One of our earlier studies explored the higher efficiency of the photocatalytic activity of the
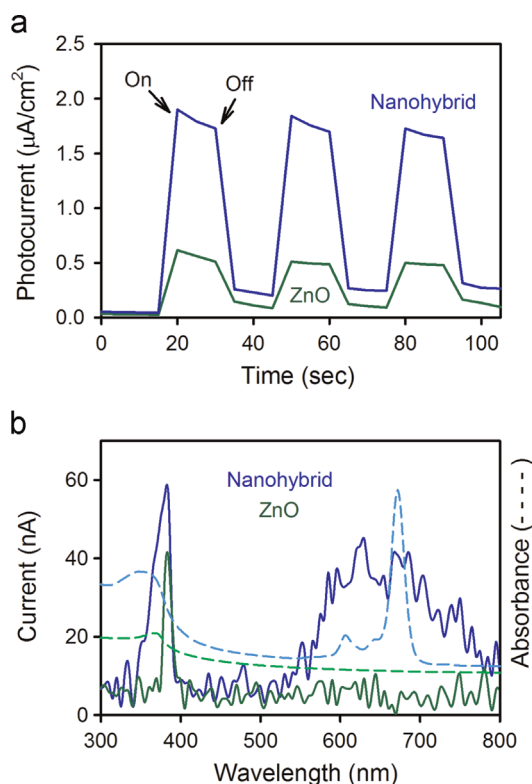
Fig. 6. (a) White light response of the nanohybrid and reference ZnO NR. A significant enhancement is observed for the nanohybrid. (b) Wavelength-dependent photocurrent spectra of the nanohybrid and bare ZnO NR (solid lines). The absorption spectra of the corresponding samples are also shown by dotted lines.
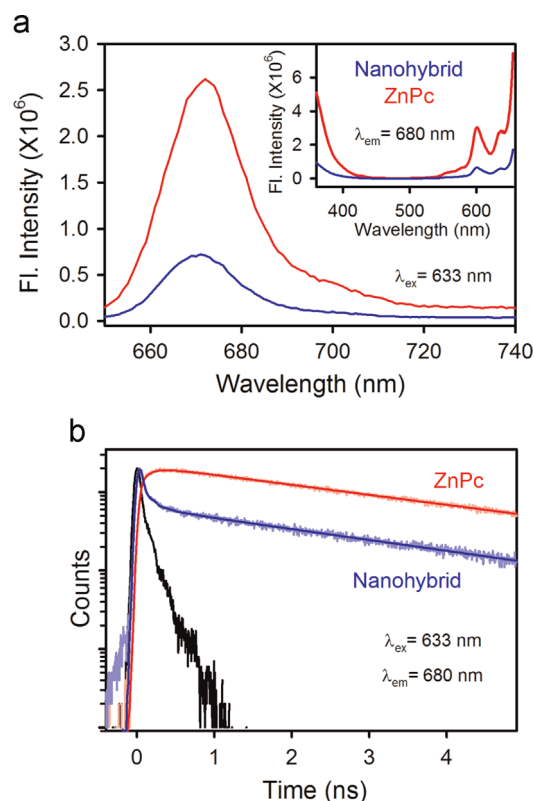

Fig. 7. (a) Steady-state emission spectra of ZnPc in DMSO and in the nanohybrids with the same concentration are shown. Fluorescence quenching of ZnPc in the nanohybrid upon 633 nm excitation is notable. Excitation spectra at a detection wavelength of 680 nm are also shown in the inset. (b) Picosecond-resolved fluorescence quenching of ZnPc in nanohybrid on glass plate compared to ZnPc in DMSO under red laser excitation (633 nm) and detected at 680 nm. Instrument response function is also shown as a reference (see text for details).

protoporphyrin-IX–ZnO nanohybrid under green light irradiation through the formation of enhanced reactive oxygen species (ROS) in the medium [22]. The ROS generation in the present case is also monitored directly by the dichlorofluorescin–dichlorofluorecein (DCFH–DCF) conversion in an aqueous medium. DCFH is a well-known marker for ROS detection [34]. ROS oxidize non-fluorescent DCFH to fluorescent DCF, and the emission intensity of the DCF was monitored with time as shown in Fig. 3d. In the presence of nanohybrids, maximum enhancement in fluorescence intensity was observed under red light irradiation. In a control experiment, ZnO NPs show insignificant ROS generation under red light illumination because the NPs lack photon absorption in the red region of the optical spectrum. It has to be noted that we cannot compare the efficacy of ROS generation of bare ZnPc as the sensitizer itself is insoluble in water. Time-dependent DCF emission in the absence of the ZnO/nanohybrid is also shown as a control experiment.

To explore the application potentiality of the nanohybrids, we have sensitized ZnO nanorods (ZnO NR) with ZnPc through the tartrate ligand and formed a flow device as shown in Scheme 1c. The SEM images of ZnO NRs used in the flow device are shown in Fig. 4a, top view and Fig. 4b, side view. The ZnO NRs are found to be 2–3 μm in length and have diameters of 80–100 nm. The synthesized NR surfaces without sensitization were found to be emitting at 590 nm due to the intrinsic oxygen vacancy in the material [35]. We have exploited FRET from the NR surface to the attached ZnPc due to their significant spectral overlap as shown in Fig. 5a. A significant quenching of the NR emission is shown in Fig. 5b. The broad NR emission is composed of two bands; One arises from the doubly charged vacancy center (V_o^{++}) located at 610 nm (P_2), and the other arises from the singly charged vacancy center (V_o^+) located at 550 nm (P_1) [36,37]. The emission intensity of ZnO NRs in the nanohybrid decreases considerably compared to

that of free ZnO NRs, which can be attributed to the efficient non-radiative photo-induced processes from ZnO NRs to the ZnPc. Herein, we propose Förster Resonance Energy Transfer (FRET) from the donor ZnO NRs to the acceptor ZnPc. The assessment of molecular distances in numerous assemblies from FRET calculations has become a very useful tool [20,38–40]. The fluorescence decay profile of the donor ZnO NRs in the presence and absence of the acceptor ZnPc were obtained upon excitation with 375 nm laser and monitored at 550 nm (P_1) and 610 nm (P_2) (Fig. 5c and d, respectively). The excited-state lifetime of the ZnO NRs quenches in the nanohybrid compared to that of bare ZnO NRs. The details of the spectroscopic parameters and the fitting parameters of the fluorescence decays are tabulated in Table 1. From FRET calculations, the distance between the donor ZnO NRs and acceptor ZnPc is determined to be 3.3 nm and 3.1 nm for the P_1 and P_2 states, respectively. The energy transfer efficiency is calculated to be 86.2% and 89.3% from the P_1 and P_2 states, respectively. This observation is consistent with the fact that P_2 (V_o^{++}) states are closer to the surface of the ZnO NR [41]. The FRET distances confirm the proximity of the ZnPc to the ZnO NRs with molecular resolution.

The photoconductivity measurement [22] of the nanohybrid film was carried out to better understand the contribution of photo-induced charge separation to the net photocurrent in the device (Scheme 1c). Fig. 6a shows the photocurrent response for the sensitized ZnO NR thin film under white light illumination. An improved photocurrent was observed for the nanohybrid thin film (∼1.8 μA) under illuminated conditions compared to the ZnO NR thin film (∼0.6 μA). The contribution of the ZnPc sensitizer to the
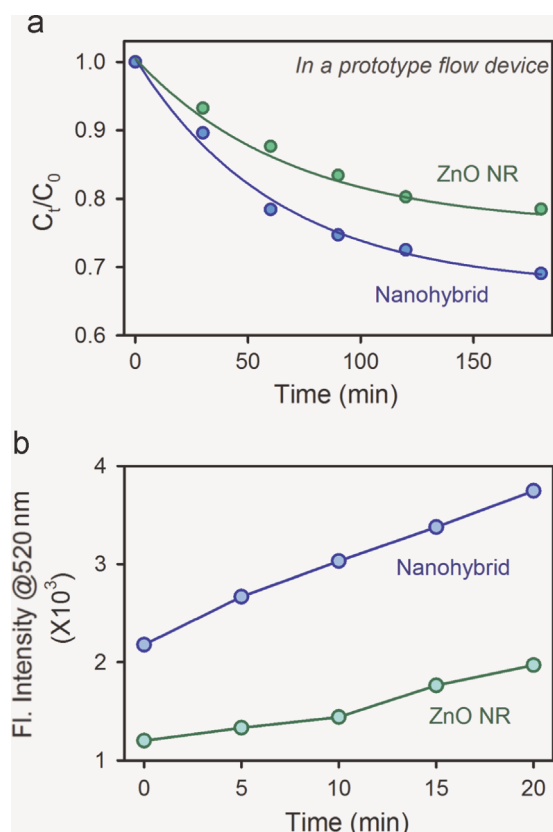
Fig. 8. Prototype performance: (a) photodegradation of MO under visible light illumination. (b) Enhanced generation of ROS in the presence of nanohybrid compared to bare ZnO NR is shown.

charge separation for better light harvesting in the near red region is evident from Fig. 6b. The wavelength-dependent photocurrents in the device format for the sensitized ZnO NR and the bare ZnO NR are consistent with the absorption spectra of the corresponding materials. In the case of the sensitized ZnO NRs, the additional peak at 650 nm in the photocurrent spectrum compared to that of the bare ZnO NR (peak at 370 nm) is in accordance with that of the 650 nm in the absorption spectrum of the nanohybrid. To investigate a molecular basis for the enhanced photocurrent in the red region of the excitation spectrum, which is close to the absorption of the sensitizer ZnPc, we have performed picosecond-resolved studies. Fig. 7a shows the steady-state emission spectra of the nanohybrid and free ZnPc in a DMSO solution. The concentration of ZnPc was maintained at the same level for both cases. A significant quenching of ZnPc emission upon red light excitation (633 nm) in the former case compared to the latter one is clearly evident from Fig. 7a, revealing excited-state electron transfer from the LUMO of ZnPc to the host ZnO NR in the nanohybrid. Direct evidence of excited-state electron transfer is revealed from picosecond resolution fluorescence transients (excitation 633 nm, Fig. 7b). One additional faster component of 30 ps (93%) in the nanohybrid emission, compared to the single exponential fluorescence decay of ZnPc in DMSO, clearly indicates an ultrafast photo-induced electron transfer in the former case [42,43]. To explore the potential application of the functional materials that have been developed here, we have made a prototype of a flow device as shown in Scheme 1c. The photocatalytic activity in the device under white light illumination ($\lambda > 365$ nm) is shown in Fig. 8a. A significant enhancement in the catalytic activity compared to that in bare ZnO NR is consistent with enhanced generation of photo-induced ROS in the device, as is evident from Fig. 8b. If the nanorods are dipped in a solution of ZnPc without tartrate ligand then during washing the dyes which

stick to the nanorods are washed out. The photocatalytic activity of the device without using tartrate ligand is found to be similar as ZnO NRs only.

4. Conclusion

In summary, we have sensitized ZnO NPs with ZnPc through a tartrate ligand for the light-harvesting application in the red region of the solar spectrum. A variety of spectroscopic and microscopic techniques have been employed to confirm the formation of a nanohybrid of ZnO with the organic ZnPc. We have used the nanohybrid for a potential application of red-light-induced photocatalysis of a model water contaminant, namely MO. In a prototype, we have demonstrated that sensitized ZnO NRs in a flow device under red light illumination work reasonably well for decontamination of the model water pollutant MO. It was confirmed that the generation of enhanced ROS as a result of ultrafast photo-induced charge separation in the sensitized nanohybrid is the reason for the intrinsic catalytic activity of the flow device under red light. This work would find relevance in harvesting in the underutilized red region of the solar spectrum.

References

[1] M. Grätzel, Recent advances in sensitized mesoscopic solar cells, Acc. Chem. Res. 42 (2009) 1788–1798.
[2] B. Oregan, M. Gratzel, A low-cost, high-efficiency solar-cell based on dye-sensitized colloidal TiO$_2$ films, Nature 353 (1991) 737–740.
[3] A. Makhal, S. Sarkar, T. Bora, S. Baruah, J. Dutta, A.K. Raychaudhuri, S.K. Pal, Role of resonance energy transfer in light harvesting of zinc oxide-based dye-sensitized solar cells, J. Phys. Chem. C 114 (2010) 10390–10395.
[4] C.-Y. Chen, J.-G. Chen, S.-J. Wu, J.-Y. Li, C.-G. Wu, K.-C. Ho, Multifunctionalized ruthenium-based supersensitizers for highly efficient dye-sensitized solar cells, Angew. Chem. Int. Ed. 47 (2008) 7342–7345.
[5] M. Garcia-Iglesias, J.-J. Cid, J.-H. Yum, A. Forneli, P. Vazquez, M.K. Nazeeruddin, E. Palomares, M. Gratzel, T. Torres, Increasing the efficiency of zinc-phthalocyanine based solar cells through modification of the anchoring ligand, Energy Environ. Sci. 4 (2011) 189–194.
[6] S.D. Oosterhout, M.M. Wienk, S.S. van Bavel, R. Thiedmann, L. Jan Anton Koster, J. Gilot, J. Loos, V. Schmidt, R.A.J. Janssen, The effect of three-dimensional morphology on the efficiency of hybrid polymer solar cells, Nat. Mater. 8 (2009) 818–824.
[7] G. Mattioli, C. Melis, G. Malloci, F. Filippone, P. Alippi, P. Giannozzi, A. Mattoni, A. Amore Bonapasta, Zinc oxide–zinc phthalocyanine interface for hybrid solar cells, J. Phys. Chem. C 116 (2012) 15439–15448.
[8] G. de la Torre, C.G. Claessens, T. Torres, Phthalocyanines: old dyes, new materials. Putting color in nanotechnology, Chem. Commun. 20 (2007) 2000–2015.
[9] L. Giribabu, C. Vijay Kumar, V. Gopal Reddy, P. Yella Reddy, C. Srinivasa Rao, S.-R. Jang, J.-H. Yum, M.K. Nazeeruddin, M. Grätzel, Unsymmetrical alkoxy zinc phthalocyanine for sensitization of nanocrystalline TiO$_2$ films, Sol. Energy Mater. Sol. Cells 91 (2007) 1611–1617.
[10] S. Mori, M. Nagata, Y. Nakahata, K. Yasuta, R. Goto, M. Kimura, M. Taya, Enhancement of incident photon-to-current conversion efficiency for phthalocyanine-sensitized solar cells by 3D molecular structuralization, J. Am. Chem. Soc. 132 (2010) 4054–4055.
[11] J. He, A. Hagfeldt, S.-E. Lindquist, H. Grennberg, F. Korodi, L. Sun, B. Åkermark, Phthalocyanine-sensitized nanostructured TiO$_2$ electrodes prepared by a novel anchoring method, Langmuir 17 (2001) 2743–2747.
[12] G. Bottari, G. de la Torre, D.M. Guldi, T. Torres, Covalent and noncovalent phthalocyanine − carbon nanostructure systems: synthesis, photoinduced electron transfer, and application to molecular photovoltaics, Chem. Rev. 110 (2010) 6768–6816.

[13] M.K. Nazeeruddin, R. Humphry-baker, M. Grätzel, D. Wöhrle, G. Schnurpfeil, G. Schneider, A. Hirth, N. Trombach, Efficient near-IR sensitization of nano-crystalline TiO$_2$ films by zinc and aluminum phthalocyanines, J. Porphyr. Phthalocyanines 03 (1999) 230–237.

[14] Ü. Özgür, Y.I. Alivov, C. Liu, A. Teke, M.A. Reshchikov, S. Doğan, V. Avrutin, S.-J. Cho, H. Morkoç, A comprehensive review of ZnO materials and devices, J. Appl. Phys. 98 (2005) 041301.

[15] S. Baruah, J. Dutta, pH-dependent growth of zinc oxide nanorods, J. Cryst. Growth 311 (2009) 2549–2554.

[16] S. Baruah, J. Dutta, Effect of seeded substrates on hydrothermally grown ZnO nanorods, J. Sol–Gel Sci. Technol. 50 (2009) 456–464.

[17] S. Sarkar, A. Makhal, K. Lakshman, T. Bora, J. Dutta, S.K. Pal, Dual-sensitization via electron and energy harvesting in CdTe quantum dots decorated zno nanorod-based dye-sensitized solar cells, J. Phys. Chem. C 116 (2012) 14248–14256.

[18] S. Sardar, S. Sarkar, M.T.Z. Myint, S. Al-Harthi, J. Dutta, S.K. Pal, Role of central metal ions in hematoporphyrin-functionalized titania in solar energy con-version dynamics, Phys. Chem. Chem. Phys. 15 (2013) 18562–18570.

[19] P. Kar, S. Sardar, E. Alarousu, J. Sun, Z.S. Seddigi, S.A. Ahmed, E.Y. Danish, O.F. Mohammed, S.K. Pal, Impact of metal ions in porphyrin-based applied materials for visible-light photocatalysis: key information from ultrafast electronic spectroscopy, Chem. Eur. J. 20 (2014) 10475–10483.

[20] J.R. Lakowicz, Principles of Fluorescence Spectroscopy, 2nd ed., Kluwer Aca-demic/ Plenum, New York, 1999.

[21] S. Sardar, P. Kar, S. Sarkar, P. Lemmens, S.K. Pal, Interfacial carrier dynamics in PbS–ZnO light harvesting assemblies and their potential implication in pho-tovoltaic/photocatalysis application, Sol. Energy Mater. Sol. Cells 134 (2015) 400–406.

[22] S. Sardar, S. Chaudhuri, P. Kar, S. Sarkar, P. Lemmens, S.K. Pal, Direct obser-vation of key photoinduced dynamics in a potential nano-delivery vehicle of cancer drugs, Phys. Chem. Chem. Phys. 17 (2015) 166–177.

[23] S. Chaudhuri, S. Sardar, D. Bagchi, S.S. Singha, P. Lemmens, S.K. Pal, Sensiti-zation of an endogenous photosensitizer: electronic spectroscopy of riboflavin in the proximity of semiconductor, insulator, and metal nanoparticles, J. Phys. Chem. A 119 (2015) 4162–4169.

[24] J. Obirai, N.P. Rodrigues, F. Bedioui, T. Nyokong, Synthesis, spectral and elec-trochemical properties of a new family of pyrrole substituted cobalt, iron, manganese, nickel and zinc phthalocyanine complexes, J. Porphyr. Phthalo-cyanines 07 (2003) 508–520.

[25] M.-S. Liao, S. Scheiner, Electronic structure and bonding in metal phthalo-cyanines, Metal=Fe, Co, Ni, Cu, Zn, Mg, J. Chem. Phys. 114 (2001) 9780–9791.

[26] G.B. Deacon, R.J. Phillips, Relationships between the carbon–oxygen stretching frequencies of carboxylato complexes and the type of carboxylate coordina-tion, Coord. Chem. Rev. 33 (1980) 227–250.

[27] A. McLaren, T. Valdes-Solis, G. Li, S.C. Tsang, Shape and size effects of ZnO nanocrystals on photocatalytic activity, J. Am. Chem. Soc. 131 (2009) 12540–12541.

[28] A. Giri, N. Goswami, M. Pal, M.T. Zar Myint, S. Al-Harthi, A. Singha, B. Ghosh, J. Dutta, S.K. Pal, Rational surface modification of Mn$_3$O$_4$ nanoparticles to induce multiple photoluminescence and room temperature ferromagnetism, J. Mater. Chem. C 1 (2013) 1885–1895.

[29] S. Ghosh, A. Priyam, S. Bhattacharya, A. Saha, Mechanistic aspects of quantum dot based probing of Cu (II) ions: role of dendrimer in sensor efficiency, J. Fluoresc. 19 (2009) 723–731.

[30] H.R. Ibrahim, M.I. Hoq, T. Aoki, Ovotransferrin possesses SOD-like superoxide anion scavenging activity that is promoted by copper and manganese binding, Int. J. Biol. Macromol. 41 (2007) 631–640.

[31] A. Zyoud, N. Zaatar, I. Saadeddin, M.H. Helal, G. Campet, M. Hakim, D. Park, H.S. Hilal, Alternative natural dyes in water purification: anthocyanin as TiO$_2$-sensitizer in methyl orange photo-degradation, Solid State Sci. 13 (2011) 1268–1275.

[32] S. Afzal, W.A. Daoud, S.J. Langford, Photostable self-cleaning cotton by a cop-per(II) porphyrin/TiO$_2$ visible-light photocatalytic system, ACS Appl. Mater. Interfaces 5 (2013) 4753–4759.

[33] S. Sardar, P. Kar, S.K. Pal, The impact of central metal ions in porphyrin functionalized ZnO/TiO$_2$ for enhanced solar energy conversion, J. Mater. NanoSci. 1 (2014) 19.

[34] C.P. LeBel, H. Ischiropoulos, S.C. Bondy, Evaluation of the probe 2',7'-dichlor-ofluorescin as an indicator of reactive oxygen species formation and oxidative stress, Chem. Res. Toxicol. 5 (1992) 227–231.

[35] A.B. Djurišić, Y.H. Leung, K.H. Tam, L. Ding, W.K. Ge, H.Y. Chen, S. Gwo, Green, yellow, and orange defect emission from ZnO nanostructures: influence of excitation wavelength, Appl. Phys. Lett. 88 (2006) 103107.

[36] K. Vanheusden, W.L. Warren, C.H. Seager, D.R. Tallant, J.A. Voigt, B.E. Gnade, Mechanisms behind green photoluminescence in ZnO phosphor powders, J. Appl. Phys. 79 (1996) 7983–7990.

[37] A. van Dijken, E.A. Meulenkamp, D. Vanmaekelbergh, A. Meijerink, The kinetics of the radiative and nonradiative processes in nanocrystalline ZnO particles upon photoexcitation, J. Phys. Chem. B 104 (2000) 1715–1723.

[38] R.M. Clegg, Fluorescence resonance energy transfer and nucleic acids, in: J.E.D. David, M.J. Lilley (Eds.), Methods in Enzymology, Academic Press, Mas-sachusetts, 1992, pp. 353–388.

[39] T. Bora, K.K. Lakshman, S. Sarkar, A. Makhal, S. Sardar, S.K. Pal, J. Dutta, Modulation of defect-mediated energy transfer from ZnO nanoparticles for the photocatalytic degradation of bilirubin, Beilstein J. Nanotechnol. 4 (2013) 714–725.

[40] S. Sarkar, S. Sardar, A. Makhal, J. Dutta, S. Pal, Engineering FRET-based solar cells: manipulation of energy and electron transfer processes in a light har-vesting assembly, in: X. Wang, Z.M. Wang (Eds.), High-Efficiency Solar Cells, Springer International Publishing, Europe, 2014, pp. 267–318.

[41] A. Makhal, S. Sarkar, T. Bora, S. Baruah, J. Dutta, A.K. Raychaudhuri, S.K. Pal, Dynamics of light harvesting in ZnO nanoparticles, Nanotechnology 21 (2010) 265703.

[42] D. Ino, K. Watanabe, N. Takagi, Y. Matsumoto, Electron transfer dynamics from organic adsorbate to a semiconductor surface: zinc phthalocyanine on TiO$_2$ (110), J. Phys. Chem. B 109 (2005) 18018–18024.

[43] J. He, G. Benkö, F. Korodi, T. Polívka, R. Lomoth, B. Åkermark, L. Sun, A. Hagfeldt, V. Sundström, Modified phthalocyanines for efficient near-IR sensitization of nanostructured TiO$_2$ electrode, J. Am. Chem. Soc. 124 (2002) 4922–4932.